Journal of Power Technologies 102 (2) (2022) 68 -- 78

Thermal-strength analysis of a slow closing valve during accelerated startup of a steam turbine

Mateusz Bryk[1,✉]

[1]Institute of Fluid-Flow Machinery Polish Academy of Sciences, 14 Fiszera street, 80-231 Gdansk, Poland
✉ mbryk@imp.gda.pl

Abstract

This study assesses the accelerated startup of a steam turbine from the perspective of a slow closing valve. Valves are one of the first components affected by high temperature gradients and are key components on which the power, efficiency and safety of the steam system depends. The authors calibrated the valve model based on experimental data and then performed extended Thermal-FSI analyses relative to the experiment. Key results of the work include the possibility to reduce the startup time of a steam turbine while complying with stress limits and not excessively straining structural components of the valve. The single most important finding is that there is no need to change valves when accelerating the startup of steam turbines.

Introduction

Every startup of a steam-based machine is a complex technical and operational issue. When starting from a cold (environment) state, the temperature of metal elements increases by several hundred degrees in just a few minutes. This is accompanied by thermal expansion of the metal and thermally induced displacements. Thus, one observes deformations of metal elements and an increase in stress in the metal, especially when backlashes between elements are too small. These phenomena occur at a different rate for hull elements and for the rotor [1, 2]. Other elongations of rotor and hull elements lead to a reduction in technological backlash and increase the risk of blurring the turbine components [3]. Frequent load changes and high heating speeds of metal parts lead to rapid thermal fatigue and material cracking. Thermal deformations can lead to permanent deformation of different metals as well as composite elements [4,5,6].

Our analysis is dedicated to the relatively novel applicability of valves [6,7]. Recently, steam valves have been used in large-scale technologies termed “power to fuel”, which are based on the rapidly expanding wind and solar energy sectors. In particular, high temperature (800-1000^{o}C), high pressure (up to 20MPa) solid oxide electrolysis cells (SOEC) have been widely applied as an effective, environmentally friendly, economically attractive and very innovative robust technologies for conversion of electrical energy into hydrogen [8,9].

From our study of environmental data [10] it is evident that wind and solar energy sources are very unpredictable in their power and frequency of usability. This fact turns our focus to making the growing share of renewable energy in the Polish power system a better partner for conventional units, which at present are having to change the nature of their work so as to fit in with renewable sources.

Concepts of effective cooperation of renewable sources with conventional sources are currently being developed in Poland. In short, the following solutions can be used to increase the flexibility of steam-based power units:

- energy stores:
  - compressed or liquid air storage [11]
  - heat stores in the steam circuit [10]
  - storage of hydrogen and hydrogen-based synthetic fuels [12, 13]
  - thermal energy storage [14]
  - electrical energy storage [15]
- advanced temperature control of stressed machine components [16, 17]
- improved efficiency of steam cycles [18,19],
- advanced modeling to determine non-design constraints using elastic-plastic material adaptation [20,21].

Previous work by the authors [21,22] demonstrated the possibility of using steam cooling to reduce by one hour the startup time of the turbine from the warm state. This procedure reduces stress in the turbine structure during the accelerated startup. Going further in this direction, the aim of this work is to determine the possibility of carrying out accelerated startup of a steam machine from the angle of slow closing valves. Earlier works state it is safe to conduct this accelerated startup solution with cooling steam injection. In addition, Siemens proposed the use of steam injection with lower parameters for cooling turbine components exposed to high temperature values [23,24].

In this paper, the authors calibrated the valve model based on the experiment of Professor Orloś. Then, having the numerically mapped model, the authors extended the analysis of the valve made in the experiment with the phenomena occurring during the accelerated startup.

Theory

Analyzed geometry

For the purposes of the analysis, the authors drew on an experiment conducted at the Military University of Technology in Warsaw (WAT) by Orłoś et al. [25]. The temperature distribution was analyzed and used to determine the distribution of stresses in the quick-closing valve. The geometry of the valve is shown in Figure 1, where its characteristic dimensions are shown.

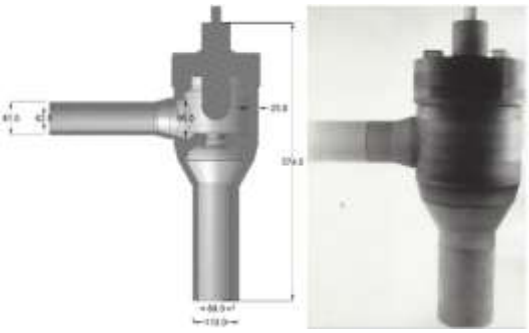

Figure 1: Main dimensions of analyzed geometry (experiment) in millimeters

The actual model is made of E-2 epoxy resin hot cast in sheet metal dies. The castings were machined, armed with sensors and then glued together with E-5 epoxy resin. Based on the available documentation, three-dimensional geometry of the valve was made (Figure 2). For the sake of simplicity, the screw connection was not reproduced in the model.

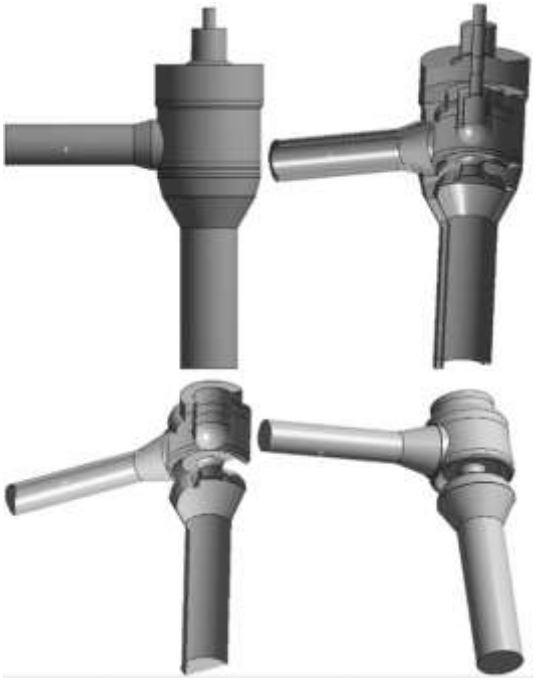

Figure 2: Solid (up) and fluid (down) domain

CFD Model

For the fluid flow simulation, three basic formulas of conservation must be fulfilled. These three main formulations, which describe CFD, are presented below [26]:

Conservation of mass equation:

$$\partial_t(\rho) + \mathrm{div}(\rho \mathbf{v}) = 0 \tag{1}$$

Conservation of momentum equation:

$$\partial_t(\rho \mathbf{v}) + \mathrm{div}(\rho \mathbf{v} \otimes \mathbf{v} + p\mathbf{I}) = \mathrm{div}(\boldsymbol{\tau}^c) + \rho \mathbf{b} \tag{2}$$

Conservation of energy equation:

$$\partial_t(\rho e) + \mathrm{div}\left[\left(e + \frac{P}{\rho}\right)\rho \mathbf{v}\right] = \mathrm{div}(\mathbf{q} + \mathbf{q}^t + \boldsymbol{\tau}^c \mathbf{v} + \mathbf{q}^D) + \rho \mathbf{b} \cdot \mathbf{v} \tag{3}$$

These are balance equations in the conservative form, where: ρ - gas density, [kg/m^3]; $\boldsymbol{\tau}^c = \boldsymbol{\tau} + \mathbf{R} + \mathbf{D}$ - total tensor of irreversible stress, [Pa] that consist molecular, turbulent and diffusive parts; $\mathbf{v} = v_i \mathbf{e}_i$ – mean velocity, [m/s]; $\mathbf{q}$ – molecular heat flux, [W/m^2];

$\mathbf{q}^t$ - turbulent heat flux, [W/m^2]; $\mathbf{q}^D$ - diffusive heat flux, [W/m^2]; p - pressure, [Pa]; $e = u + \frac{1}{2}\mathbf{v}\cdot\mathbf{v}$ - specific total energy, [J/kg]; $\mathbf{b} = -9{,}81\mathbf{e}_z$ [m/s^2].

Additionally, the above set of three governing equations, i.e. (1-3), were complemented by two evolution equations for parameters, which were used to define turbulent tensor $\mathbf{R}$ components [26]. The first is the evolution equation concerning turbulent energy k (4):

$$\partial_t(\rho k) + \mathrm{div}(\rho k\mathbf{v}) = \mathrm{div}(\mathbf{J}_k) + S_k \quad (4)$$

The second one is the evolution equation concerning energy dissipation ε (5):

$$\partial_t(\rho\varepsilon) + \mathrm{div}(\rho\varepsilon\mathbf{v}) = \mathrm{div}(\mathbf{J}_\varepsilon) + S_\varepsilon \quad (5)$$

CSD Model

In order to solve the solid state problem, basic equations used in CSD simulations and equation governing species transport are used [21,22,26]. Please note that a common form of CFD and CSD is required since during numerical simulations there is a need for simultaneous calculations and numerous exchanging of fluid and solid resulting data. Therefore, with respect to CSD one must start from the following "conservation form" of CSD [27]:

$$\frac{\partial}{\partial t}\begin{Bmatrix}\rho\\ \rho\mathbf{v}\\ \rho e\\ \rho\boldsymbol{\varepsilon}^{\mathrm{pl}}\\ \rho\boldsymbol{\alpha}\\ \rho r\end{Bmatrix} + \mathrm{div}\begin{Bmatrix}\rho\mathbf{v}\\ \rho\mathbf{v}\otimes\mathbf{v}\\ \rho e\mathbf{v}\\ \rho\boldsymbol{\varepsilon}^{\mathrm{pl}}\otimes\mathbf{v}\\ \rho\boldsymbol{\alpha}\otimes\mathbf{v}\\ \rho r\mathbf{v}\end{Bmatrix} = \mathrm{div}\begin{Bmatrix}0\\ \boldsymbol{\sigma}\\ \boldsymbol{\sigma}\,\mathbf{v}+\mathbf{q}^{\mathrm{c}}\\ 0\\ 0\\ \mathbf{J}_{\mathbf{r}}\end{Bmatrix} + \begin{Bmatrix}0\\ \rho\mathbf{b}\\ \rho S_{\mathrm{e}}\\ \rho\mathbf{S}_{\mathrm{pl}}\\ \rho\mathbf{S}_{\alpha}\\ \rho S_{\mathrm{r}}\end{Bmatrix} \quad (6)$$

Thermal-FSI tools

Thermal-FSI analysis consists in CFD analysis, the results of which are exported to a solid state solver (CSD). Next, the CSD solver on the basis of imported data (temperature, pressure) determines the stress and displacements in the analyzed geometry. The principle of the analysis is shown schematically in Figure 3.

In the literature, there are two types of Thermal-FSI [22,28] analysis: one way FSI and two way FSI. There is a difference to the momentum-FSI where, in one way FSI, after CFD calculations, the solution of the pressure field is exported to the CSD solver and used to determine the stress and displacements. In one way thermal-FSI, the cooling or heating of fluid by a solid body is realized with the Neumann type boundary conditions.

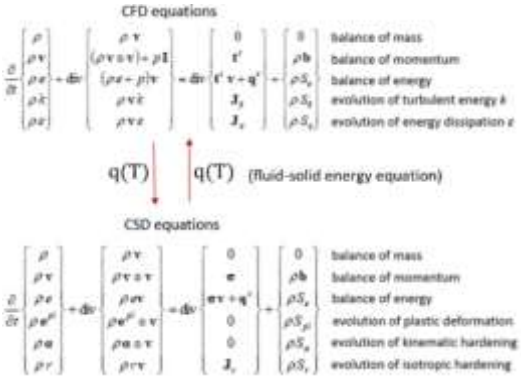

Figure 3: Principle of operation of the Thermal-FSI [28]

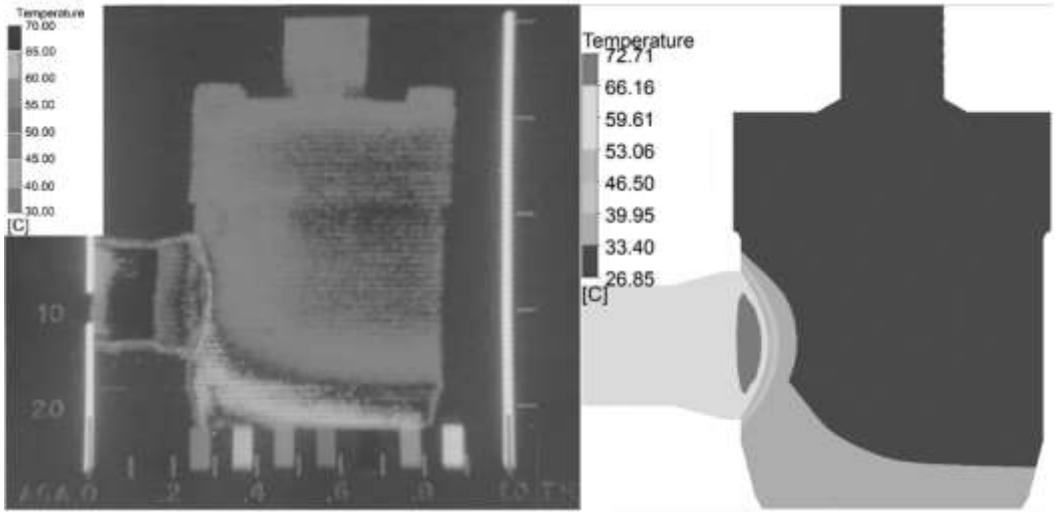

Figure 4: Temperature distribution - 20 min after startup. Left, experiment; right, Thermal-FSI

In the case of two-way Thermal-FSI analysis, the CFD and CSD models are coupled together during the entire simulation through the energy equation balance. To be precise, this coupling takes place on a common surface between the solid and fluid domain, where the crucial boundary condition is (7) [29]:

$$(\mathbf{q} + \mathbf{q}^t + \mathbf{q}^{rad} + \mathbf{q}^D) \cdot \mathbf{n}_{|solid} + (\mathbf{q} + \mathbf{q}^t + \mathbf{q}^{ph}) \cdot \mathbf{n}_{|fluid} = 0 \,. \quad (7)$$

The work involved two-way Thermal-FSI analyses. Temperature fields were automatically imported: from solid to fluid and, vice versa, from fluid to solid. Finally, from the field of temperature, a new pressure in the fluid state and new thermal stress fields in the solid state were determined in the analyzed numerical domain.

FVM discretization of the simulation domain

The valve's 3D geometry was discretized using the finite volume method (FVM). Both the liquid and solid were discredited using triangular volumes. A wall layer was used. The calculation domain consists of 4 million elements for the fluid and 4.5 million for the solid. The grid of both liquid and solid is shown in Figure 4.

Experiment description

In the experiment, the valve was heated by air at atmospheric pressure from the laboratory temperature $T_0 = 24$°C up to the temperature of hot air equal to $T_{air} = const = 81$°C. A real gas model was used$c = 60$ This means that the inlet data was set at a constant speed and temperature: [OBJ]m/s and 81°C for 1 h. The inlet set parameters were constant in time and, on the external wall of the valve, a condition of natural convection was set at a constant ambient temperature of 24°C.

The experiment consisted of the following stages: making a model valve made of epoxy resin; application of the thermovision apparatus for testing stationary and transient temperature fields on the valve surface (Figures 7-9); post-determination of mass-rates, steam velocities, and heat transfer coefficients; determination of the thermal stresses by means of the reconstructed field of temperature. The domain contains 98 sensors (Figure 5). More information can be found in [47].

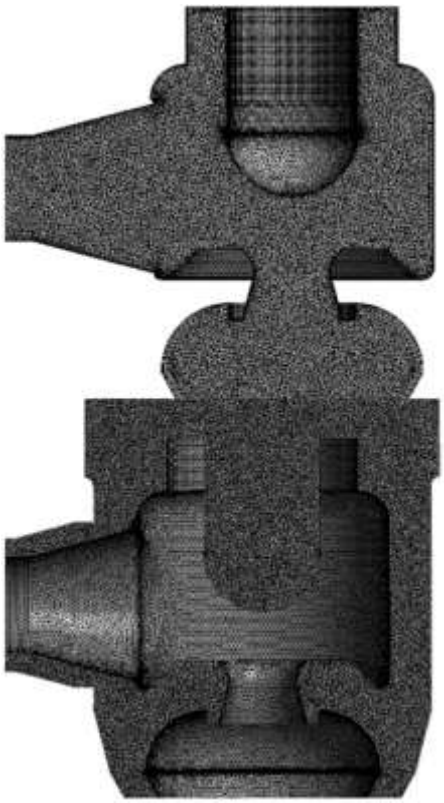

Figure 5: Liquid (up) and solid (down) FVM discretization mesh

Analysis of a full-scale valve model

Drawing on the previous WAT-epoxy experiment, the valve was re-modelled in such a manner that its geometry was scaled up four times to match the size of the actual valve. The purpose of the analysis was to check the valve's behavior under accelerated steam machine startup conditions. This is important since the literature contains data on various operating damage to valves (Jalali and Amiri [3]).

Steam tables are used for CFD modeling. The boundary conditions for flow are the pressure and temperature as at the turbine inlet during startup 3 h and 2 h. The curves of the above-mentioned parameters are shown in Fig. 6. At the outlet of the domain, pressure and temperature parameters were set based on stationary calculations. On the external wall of the valve, the condition was set of natural convection at the ambient temperature of 24°C.

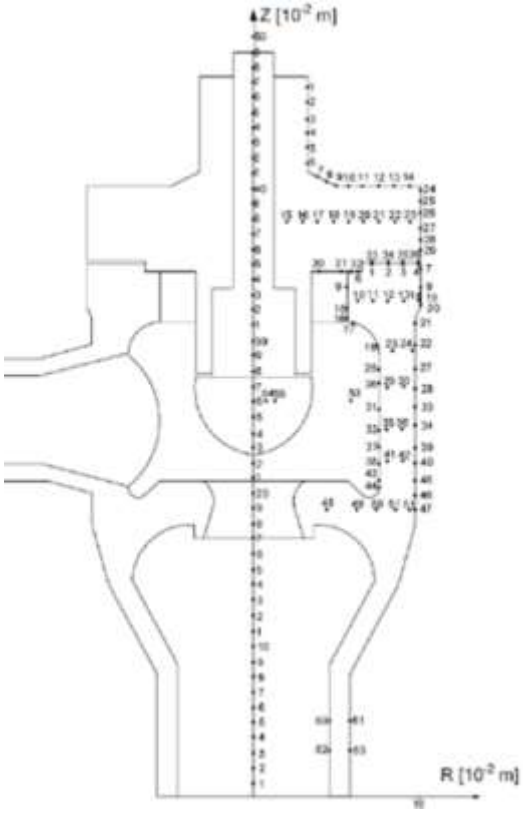

Figure 6: Axial plane of the valve with visible sensor armature [25]

The CFD and CSD models are the same as aforementioned.

Results

Temperature field distribution for air and epoxy

This sub-section presents the distribution of temperature fields on the valve surface and in characteristic planes of the analyzed geometry. The results obtained were compared with the experiment. A comparison of temperature distributions is shown in Figures 7 to 9.

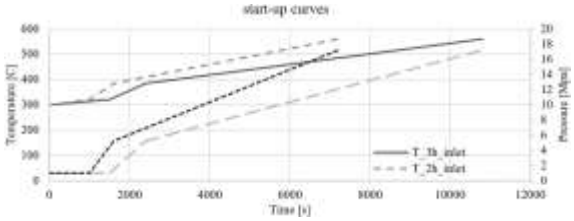

Figure 7: Steam pressure and temperature as a function of time during two startups (2 h and 3 h)

It follows that the Thermal-FSI calculations are well aligned with the thermal imaging performed in the experiment. The highest temperature values are observed on the outer surface of the intake channel. After 1 hour, the temperature is redistributed, and the established heat exchange is reached.

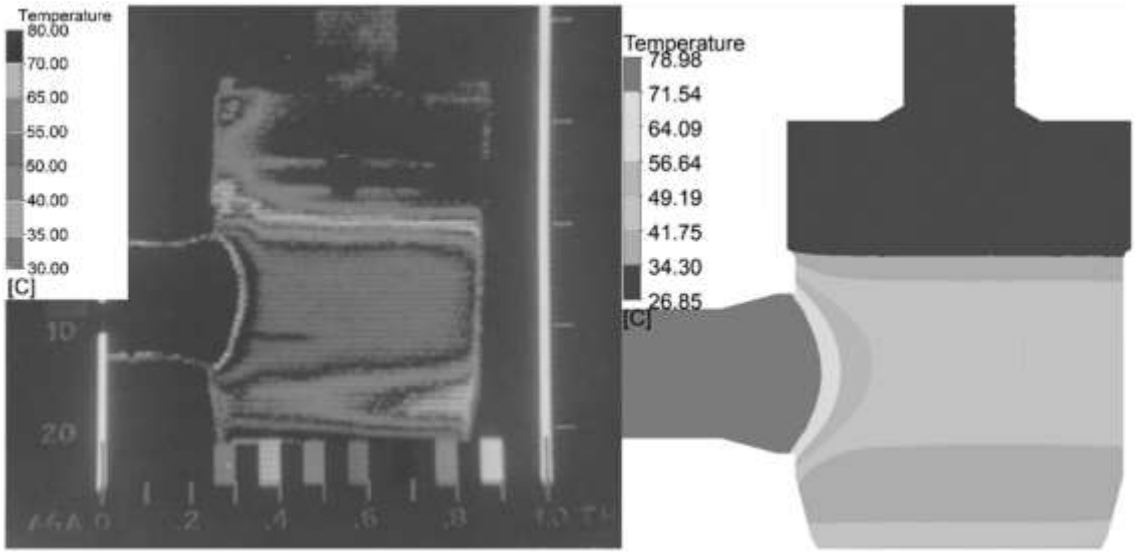

Figure 8: Temperature distribution - 60 min after startup. Left, experiment; right, Thermal-FSI

Thermal stress distribution for the epoxy and steel valve model

The results were compared to the main stresses:

σ_b – bending stress,

σ_s – shear stress,

σ_t – tensile stress.

Note that stress values were obtained after 1 h measurements (nearly stationary case). The data for the WAT-epoxy experiment (epoxy and metal) were compared with stress values determined by our CSD method.

Figure 10 shows the shear, bending, and tensile stress values in the P1 cross-plane of the epoxy model in the hot state (after 1 h). Shear stress dominates for small x-coordinate values. They reach values of up to -0.9MPa in the case of the experiment and up to -1.0MPa according to Thermal-FSI. As we move away from the hot wall, these stresses change their return, and their value exceeds 1.4 MPa for the experiment and 1.1MPa for Thermal-FSI. WAT-epoxy bending stresses reach a maximum of 0.36MPa and are highest for $x = 5$ mm. As the x value increases, the stress falls to about 0 MPa. A similar situation occurs for Thermal-FSI bending stress, but the difference is in stress values; for Thermal-FSI the bending stress takes a smaller value. Tensile stresses reach a maximum of -1.2MPa for the experiment and -1.15MPa for Thermal-FSI calculations. Figure 11 shows the stress distribution for the steel model. The highest stress occurs at the measuring points furthest away from the hot wall ($x = 94$ mm), and these are shear stresses. They reach 35 MPa for the WAT model and 30MPa for Thermal-FSI. The maximum tensile stress reaches the level of -11.0MPa for WAT-Steel and -12MPa for Thermal-FSI. The bending stresses reach a maximum of 10 MPa for WAT-Steel and 6.5MPa for Thermal-FSI for the measuring point closest to the hot $x = 0$ mm wall. The differences between WAT-steel and CSD are shown in terms of stress values.

Temperature change during startup for the full-scale steel valve model

In the first stage of modeling, the temperature distributions in the solid were determined. Figures 12–14 shows the temperature fields for the design startup (3 h) and accelerated startup (2 h). For the design startup, the temperature field schedules are shown for three time steps (100, 4500, and 10800s). For the accelerated startup, field schedules are shown for three time steps: 100, 4500, and 7200s. Individual temperature scales are used in the drawings, which emphasize the maximum temperatures. Let us note that the temperature field distributions are similar to those obtained by Li et al. in [8]. In each time step, for both start times, the highest temperature occurs in the nozzle. This is the element that heats up the fastest from the flowing air. Then, the jammer connecting the outlet pipe to the valve chamber heats up; the walls of the valve chamber are colder due to cooling on the outside of the valve. For the 100s time step, there is no difference between the maximum temperatures for 2h and 3h startups. The temperature difference is 17K for step 4500s and 31K at the end of both startup processes.

Thermal stress during startup for the full-scale steel valve model

On the basis of the obtained temperature field distributions, the stresses occurring in the valve were determined. The results are shown in the diagram in Figure 15.

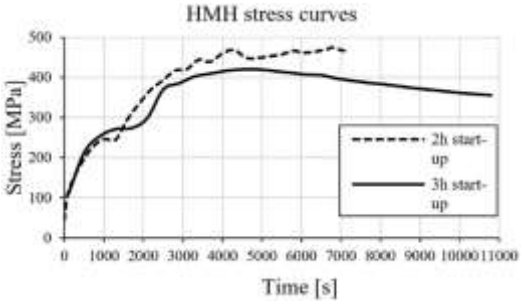

Figure 9: Comparison of HMH-equivalent stress curves during 2 h and 3 h startup.

The stress waveform for the 3h startup is standard for this type of case. After reaching the temperature value and adequate annealing of the geometry, the stresses decrease in value. The maximum stress value is 420MPa.

In the case of a 2h startup, higher temperature gradients are present in the geometry, which have an influence on the thermal stress. In this case the geometry is heated to a lesser extent than for the 3h startup, which results in the fact that the stress value at 2h does not decrease compared to the earlier time,

as it does for the 3h startup. The highest stress value is 468MPa.

At the final stage of startup, the stress takes the value of 391MPa for 3h startup and 468MPa for 2h startup.

Summary/Conclusions

The paper presents the results of numerical modeling in terms of stress distribution in the components of the slow closing valve for the design startup (3h) and accelerated (2h) steam turbine. The model was validated on the example of the WAT-experiment using a valve made of epoxy resin in 1:4 scale. After validation of the model, a full-size valve made of ST12t steel was subjected to numerical analysis. In the case of project startup, the maximum stress (HMH) occurs after 4500s and is 420MPa.

We have the following conclusions:

- in the case of accelerated startup, these stresses reach local peaks of 469MPa, 467MPa and 475MPa for 4300s, 5800s and 6800s respectively;

- the maximum stresses have been shown to increase from 400MPa for design startup (for t=4500s) to 558MPa for accelerated startup (for t=7200s);

- for the analyzed accelerated startup the maximum stresses did not reach the yield point of steel ST12t (Yield point Re >700MPa [30]), which is an important conclusion of the analysis;

- the temperature gradient increases in value twice for 2h startup in comparison with 3h startup;

- in spite of the higher value of the stress at the accelerated startup, it does not influence the safety of the valve operation;

- additional fatigue analyses should be carried out in order to estimate the influence of frequent changes of thermal load on valve construction.

There is great interest in valves connected with re-SOC technology [6] which needs fresh steam with high thermodynamic parameters. This technology needs large-scale steam storage, which is envisioned as a key requirement in modernizing and increasing flexibility in the Polish national electric grid. Since electrical energy storage is expected to play a crucial role in the near future (by 2030), accelerated startups and shutdowns will become increasingly important, as they are fundamental elements in technologies based on intermittent renewable sources such as wind and solar [9].

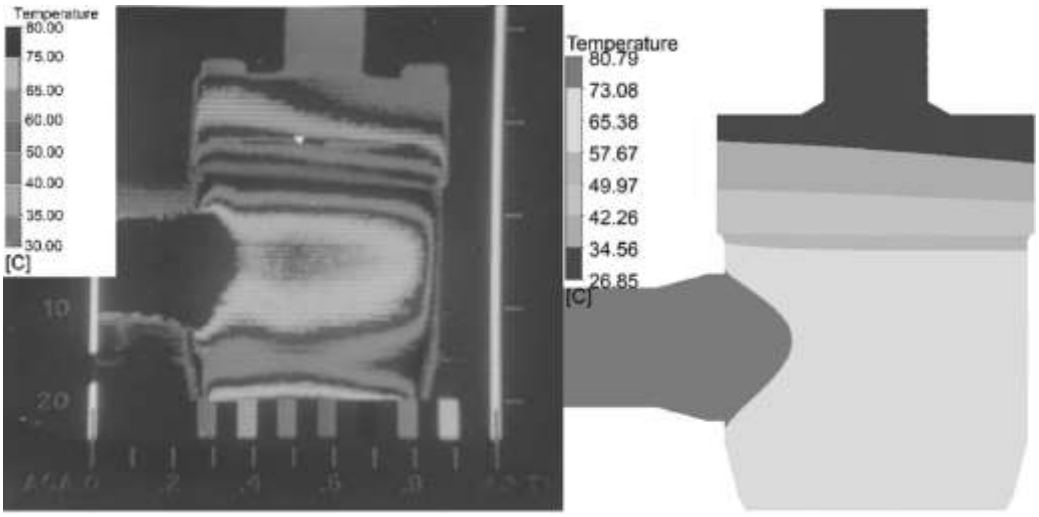

Figure 10: Temperature distribution - 3 min after startup. Left, experiment; right, Thermal-FSI

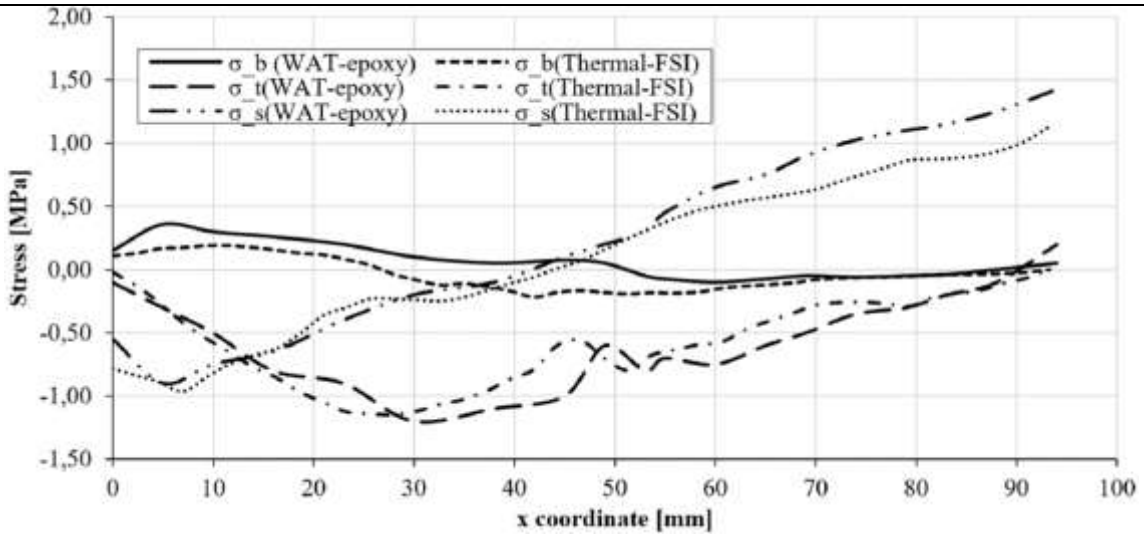

Figure 11: Stress curves, after 1 h, at P1 cross-plane. Comparison of WAT-epoxy date with CSD calculations. Indexes: σ_b – bending stress, σ_s – shear stress, σ_t – tensile stress.

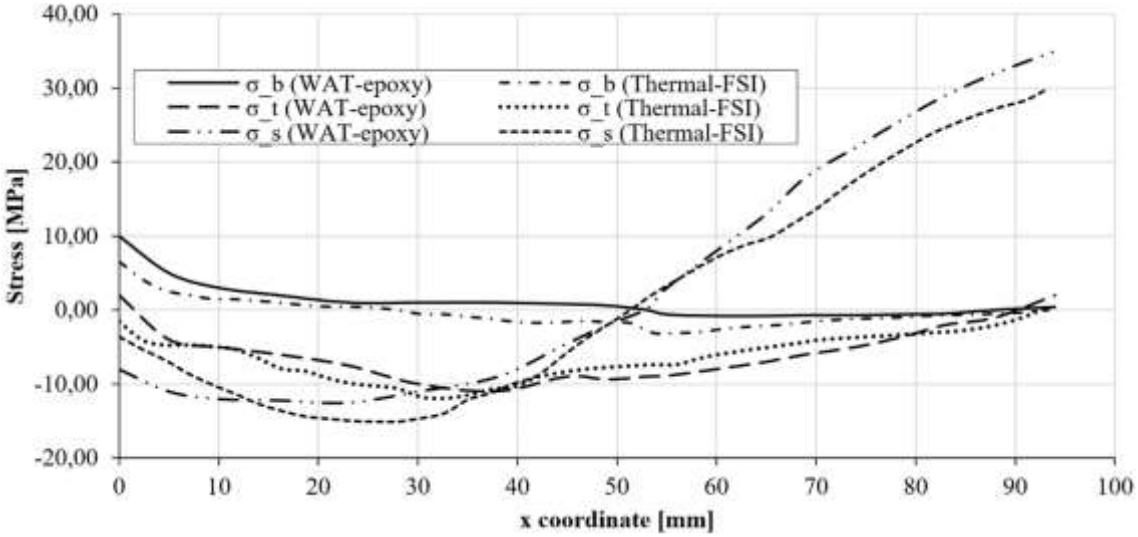

Figure 12: Stress curves after 1 hour at P1 cross-plane. Comparison of WAT-steel data with CSD simulations. Indexes: σ_b – bending stress, σ_s – shear stress, σ_t – tensile stress.

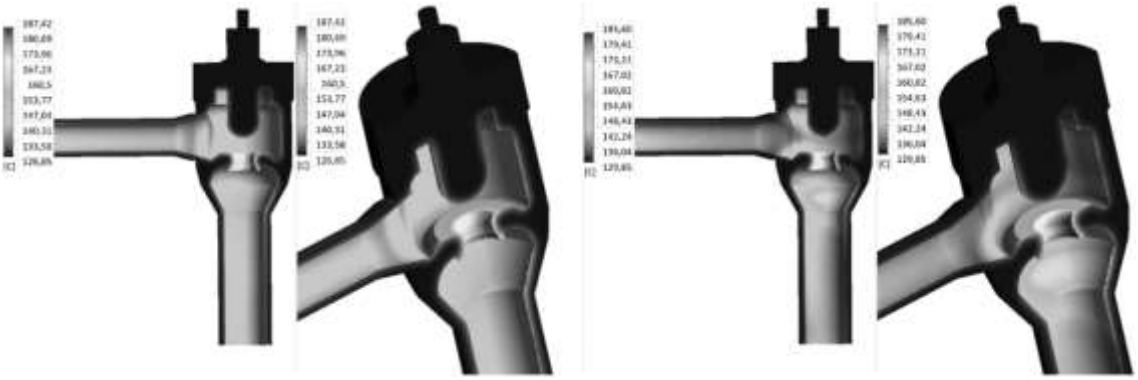

Figure 13: Temperature field distribution for time 100s. Design startup (3h) (left) and accelerated startup (2h) (right)

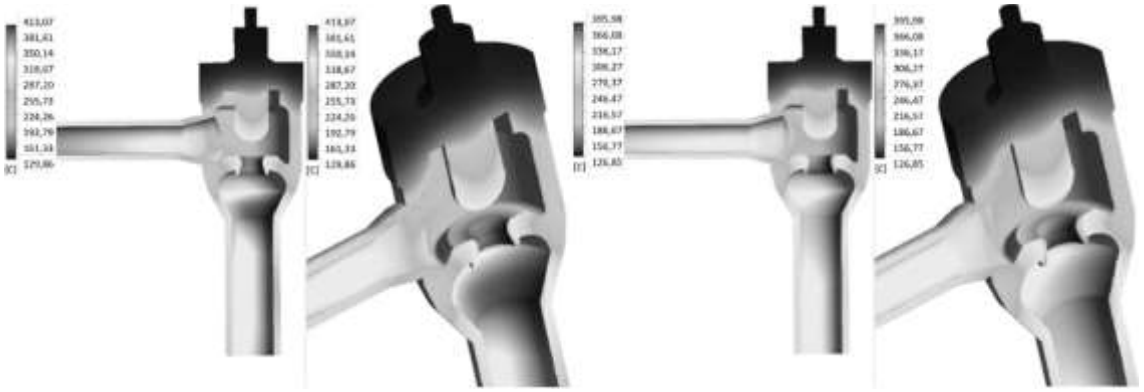

Figure 14: Temperature field distribution for time 4500s. Design startup (3h) (left) and accelerated startup (2h) (right)

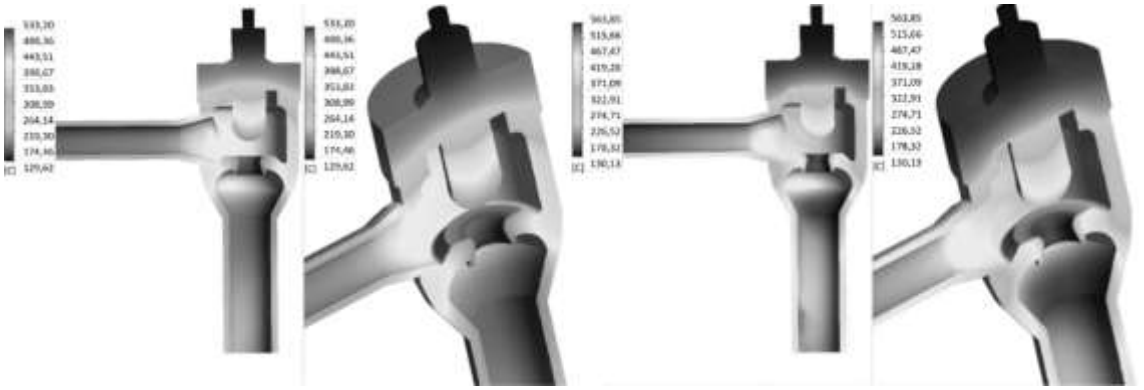

Figure 15: Temperature field distribution for time 10800s during 3h startup (left). Temperature field distribution for time 7200s during accelerated startup (right).References

References

[1] Banaszkiewicz M. Steam turbines start-ups principles of steam turbines start-ups. Transactions of the Institute of Fluid Flow Machinery 2014;126:169–198.

[2] Banaszkiewicz M. On-line monitoring and control of thermal stresses in steam turbine rotors. Applied Thermal Engineering 2016;94:763–776. doi:10.1016/j.applthermaleng.2015.10.131.

[3] Jalali A, Amiri Delouei A. Failure analysis in a steam turbine stop valve of a thermal power plant. Engineering Failure Analysis 2019;105:1131–40. doi:10.1016/j.engfailanal.2019.07.057.

[4] Li F, Quay B, Wang P, Santavicca D.A, Wang W, Xu S. Transient thermal behaviors of a scaled turbine valve: Conjugate heat transfer simulation and experimental measurement. Int. J. Heat Mass Transf 2019;141:116–28. https://doi.org/10.1016/j.ijheatmasstransfer.2019.06.053.

[5] Issues of design and operation of boilers and turbines for supercritical coal units. Gliwice: Publishing House of the Silesian University of Technology, 2010, Kosman G, Rusin A, Taler J, Pawlik A.

[6] Bryk M. Thermal-FSI analysis of rapid start-up of key components of thermal energy cycles in terms of cooperation with rSOC installation. 8th Wdzydzeanum Workshop on Fluid-Solid Interaction, U Grzegorza, Wdzydze Kiszewskie, Aug. 30-Sep. 3, 2021, Poland.

[7] Badur J, Lemański M, Kowalczyk T, Ziółkowski P, Kornet S. Zero-dimensional robust model of an SOFC

with internal reforming for hybrid energy cycles. Energy 2018;158:128-138.

[8] Kotowicz J, Jurczyk M, Węcel D, Ogulewicz W. Analysis of Hydrogen Production in Alkaline Electrolyzers. Journal of Power Technologies 2016;96:149-156.

[9] Hyrzyński R, Karcz M, Lemański M, Lewandowski K, Nojek S. Complementarity of wind and photovoltaic power generation in conditions similar to Poland. Acta Energetica 2013;17:14–21. doi:10.12736/issn.2300 3022.2013402.

[10] Kowalczyk T, Badur J, Ziółkowski P, Kornet S, Banaś K, Ziółkowski P.J. The problem of thermal plant flexibility under the conditions of dynamic RES development. Acta Energetica 2017;31:116–26. doi:10.12736/issn.2300-3022.2017209.

[11] Milewski J, Dadyda K, Szabłowski Ł. Compressed Air Energy Storage Systems. Journal of Power Technologies 2016;96:245-260.

[12] Kowalczyk T, Badur J, Bryk M. Energy and exergy analysis of hydrogen production combined with electric energy generation in a nuclear cogeneration cycle. Energy Conversion and Management 2019;198. doi:10.1016/j.enconman.2019.111805.

[13] Lepszy S, Chmielniak T, Mońka P. Storage system for electricity obtained from wind power plants using underground hydrogen reservoir. Journal of Power Technologies 2017;97:61-68.

[14] Jurczyk M., Rulik S., Bartela Ł.: Thermal energy storage in rock bed – CFD analysis. Journal of Power Technologies 2020;100:301-307.

[15] Nikolaidis P., Poullikkas A.: A comparative review of electrical energy storage systems for better sustainability. Journal of Power Technologies 2017;97:220-245.

[16] Ziółkowski P, Badur J, Ziółkowski P.J. An energetic analysis of a gas turbine with regenerative heating using turbine extraction at intermediate pressure - Brayton cycle advanced according to Szewalski's idea. Energy 2019;185:763-786. https://doi.org/10.1016/j.energy.2019.06.160

[17] Ziółkowski P, Kowalczyk T, Lemański M, Badur J. On energy, exergy, and environmental aspects of a combined gas-steam cycle for heat and power generation undergoing a process of retrofitting by steam injection. Energy Conversion and Management 2019;192:374–384.

[18] Ziółkowski P, Kowalczyk T, Kornet S, Badur J. On low-grade waste heat utilization from a supercritical steam powerplant using an ORC-bottoming cycle coupled with two sources of heat. Energy Conversion and Management 2017;146:158-173. 173.https://doi.org/10.1016/j.enconman.2017.05.028

[19] Kowalczyk T, Badur J, Ziółkowski P. Comparative study of a bottoming SRC and ORC for JouleeBrayton cycle cooling modular HTR exergy losses, fluid-flow machinery main dimensions, and partial loads. Energy 2020;206. https://doi.org/10.1016/j.energy.2020.1180723

[20] Dudda W., Bryk M., Banaszkiewicz M., Badur J.: On a comparison of Huber-Mises-Hencky with Zawadzki equivalent stress for a steam turbine blade during nonstationary thermal load. AIP Conf Proc 2020;2239. https://doi.org/10.1063/5.0007831.

[21] Badur J, Bryk M. Accelerated start-up of the steam turbine by means of controlled cooling steam injection. Energy 2019;173:1242–55. https://doi.org/10.1016/j.energy.2019.02.088.

[22] Badur J, Bryk M. Thermal-FSI modeling of the steam turbine accelerated start-up by means of cooling steam injection control. Journal of Power Technologies 2020;100:115–119.

[23] Wieghardt K. Siemens Steam Turbine Design for AD700 Power Plants. AD700 Copnference Milan, 2015.

[24] Arrel D. Next Generation Engineered Materials for Ultra Supercritical Steam Turbines. Final Technical

Report, Siemens Orlando, 2006.

[25] Orłoś Z, Augustyn M, Dobrociński S, Leitner P, Tomaszewski K. Experimental studies of temperature fields, deformation and stress state under stationary and non-stationary heat loads. Theoretical calculations of thermal stress. Warsaw Military University of Technology, 1980 (in Polish).

[26] Pięć wykładów ze współczesnej termomechaniki płynów. Wydawnictwo IMP PAN w Gdańsku, 2005, Badur J.

[27] Ziółkowski P.J, Ochrymiuk T, Ermeyev V.A. Adaptation of the arbitrary Lagrange–Euler approach to fluid–solid interaction on an example of high velocity flow over thin platelet. Continuum Mechanics and Thermodynamics 2021;33:2301-2314.

[28] Kornet S, Ziółkowski P, Jóźwik P, Ziółkowski P.J, Stajnke M, Badur J. Thermal-FSI modeling of flow and heat transfer in a heat exchanger based on minichanels. Journal of Power Technologies 2018;97:373-381.

[29] Badur J, Ziołkowski P, Kornet S, Kowalczyk T, Banaś K, Bryk M, Ziółkowski P.J, Stajnke M. Enhanced energy conversion as a result of fluid-solid interaction in micro and nanoscale. Journal of Theoretical and Applied Mechanics 56:329-32.

[30] Nikonowicz Ł, Milewski J. Determination of electronic conductance of solid oxide fuel cells. J Power Technol 2011;91:82–92.